Chapter 10

Wet – Chemically Etched Silicon Nanowire Solar Cells: Fabrication and Advanced Characterization

Björn Hoffmann, Vladimir Sivakov,
Sebastian W. Schmitt, Muhammad Y. Bashouti,
Michael Latzel, Jiří Dluhoš, Jaroslav Jiruse and
Silke Christiansen

Additional information is available at the end of the chapter

http://dx.doi.org/10.5772/52585

1. Introduction

In the past decade the usage of solar energy production has increased rapidly and has become a reasonable alternative to fossil energy sources. Solar energy conversion is a challenge of the millennium and solar cells are one eagerly thought way of converting solar energy into electrical energy. Solar cells are divided into three generations according to Martin Green [1]: The 1st generation (1st gen) is till to date dominating production and installation and makes use of bulk, essentially silicon wafers with planar cell geometry. Today, a typical silicon based cell uses 200μm thick Si wafers as substrates. The 2nd generation (2nd gen) uses thin-films rather that bulk wafers and materials can be wide spread. The idea is to use only very thin layers of photovoltaically active material on a passive mechanically supporting material e.g. glass. Such cells offer the option to use cheap substrates and even flexible substrates [2] so that cost saving potentials as well as new applications can be envisaged. Until today, thin-film cells (2nd gen) do not live up to their full potential due to the fact that they are 50%-60% less efficient than wafer cells (1st gen). Solar cell concepts termed 3rd gen aim at the combination of low production costs and high efficiencies. In order to reach this goal, unique optical and physical properties of complex nanostructures as well as novel materials and compounds are exploited. Silicon nanowires (SiNWs) are a very promising candidate for next generation PV. The basic material is abundant and cheap and the semiconductor industry gained intense experience with its handling. The nanostructuring and cell preparation can also be performed in cheap and large scale processes. Thus it could easily be integrated into existing PV lines.

1.1. Reasons for nanowires in PV concepts

The conversion efficiency of solar cells is affected by many factors. The internal quantum efficiency is already quite good for a long time and thus the industry concentrated more on optimizing the contacts for efficiency enhancement or reducing the overall costs. Whereas one efficiency record follows another in research [3], industry scale solar cells, however, are only improving slowly [4]. While optimizing factors like contact resistance or quantum efficiency only permit a moderate overall efficiency enhancement, the optical absorption is a property that can encourage large improvements of the SC efficiency. By using silicon nanostructures, the absorption of sunlight can be improved from typically 60% to over 90% in the wavelength range between 400 and 1100 nm [5–9]. This increased absorption is very encouraging and makes the nanostructures so interesting for SC research as well as for future industrial production.

One of many ways in order to reach this increased absorption of sunlight is the use of nanowires constituting the SC absorbers. The nanowires act as light trapping specimens due to its strong scattering capacities [10] and for the same reason as antireflective coatings [11–13]. A lot of different methods exist that produce such highly absorbing nanostructures which are divided into bottom-up growth mechanisms [14–16] and top-down etching processes [17–20]. This work will concentrate on a metal assisted wet-chemical etching (MA-WCE) process that does not need any vacuum equipment and can be performed even on large surfaces in a few minutes.

The application of micro- and nanowires in SCs is quite a new field of PV research. Having used the "Web of Knowledge" search engine, graphs were generated which are presented in Figure 1[1]. From the first publication in 2002 [21], the topic has rapidly increased in popularity and it has reached nearly 250 publications in 2011. The number of citations also shows a growing increase of nearly 5000 citations in 2011.

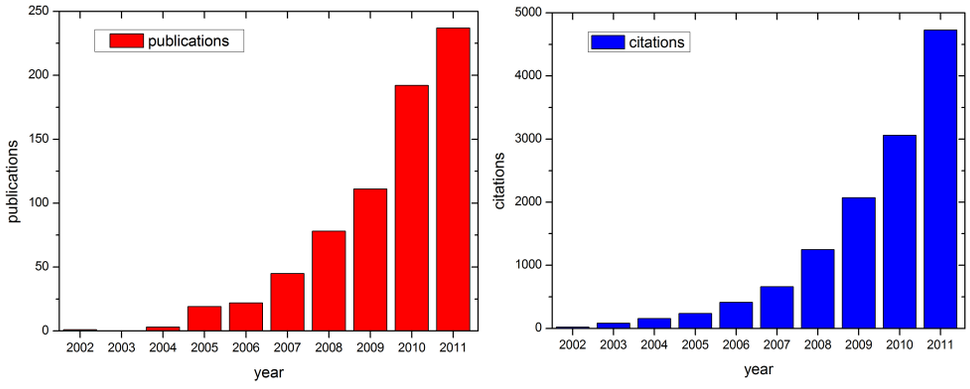

Figure 1. Publications and citations on nanowire-based solar cells in the last 10 years.

1 http://www.webofknowledge.com/ Search properties: title includes (nanowire OR nanorod OR microwire OR microrod) AND (solar)

http://dx.doi.org/10.5772/52585

2. Experimental part

2.1. Top-down fabrication of silicon

SiNWs can be produced by many different methods, normally divided into bottom-up growth mechanisms and top-down etching processes. While growing of SiNWs normally is conducted by using the vapor-liquid-solid (VLS) mechanism [14], which needs high temperatures, toxic gases and expensive vacuum equipment, top-down etching can be performed in easier ways. One differentiates between physical (dry) and chemical (wet) etching. Physical or dry etching is usually conducted in reactive gases offered in a reactive ion etching (RIE) setup [22], while chemical etching is usually based on wet chemistries, preferably on the basis of hydrofluoric acid for the case of silicon. Both methods have assets and drawbacks, but when it comes to the question of fast and cost-effective fabrication with the perspective of mass production, wet-chemical (WC) etching is intriguing.

Since details of WC etching processes were already discussed in a previous Intech book chapter [20], this work will only give a short summary and point out the latest optimization processes. The SiNW substrates that constitute the SC absorber are fabricated in a two-step MA-WCE procedure. Therefore, the substrate material, which is typically a lowly doped (1-5 Ohmcm) n-type Si wafer, passes four different etching solutions. In the beginning, the native oxide is removed with 2% hydrofluoric acid (HF, solution I). In the following step (solution II), silver (Ag) nanoparticles are formed on the surface of the wafer in a mixture of 0.02 molar (M) $AgNO_3$ and 5M HF in a ratio of 1:10. The duration of this step influences the density of particles and thus also the forming SiNW geometry. This procedure needs to be less than 30 seconds. Otherwise, the Si is completely coated by a continuous Ag layer and no access of the etching solutions to the Si surface can be achieved. Controlled SiNW properties can be achieved when using the following etching steps. Solution III consists of a mixture of 5M HF and 30% H_2O_2 in a ratio of 1:1. In this step the Si is oxidized by the interplay of H_2O_2 and the nanoscale Ag particles that form the thermodynamically unstable intermediate compound AgO(OH) which is a very efficient oxidant that oxidizes the silicon beneath the Ag nanoparticle. The resulting SiO_2 is dissolved by the HF in the solution. Thus, the Si is removed below the Ag particles which dig into the Si wafer and thus move away from the wafer surface inducing the SiNW formation. The direction of this Ag nanoparticle movement is anisotropic following certain crystal orientations and depends on the temperature as well [20]. Under controlled conditions, the SiNWs form perpendicularly to the surface of a Si(100) wafer and are oblique to the surface of a Si(111) wafer following <100>-directions [18]. In the last step (solution IV), concentrated nitric acid is used to remove the remaining Ag nanoparticles. Figure 2 illustrates the etching steps process.

During the SiNW formation, an increasing absorption can be observed after a few seconds. The shiny Si wafer surface turns matt finished and changes to a brown color which becomes deep black after one minute of etching. After three minutes the SiNWs reach a length of 1μm and elongate with a rate of 1 μm/min after that.

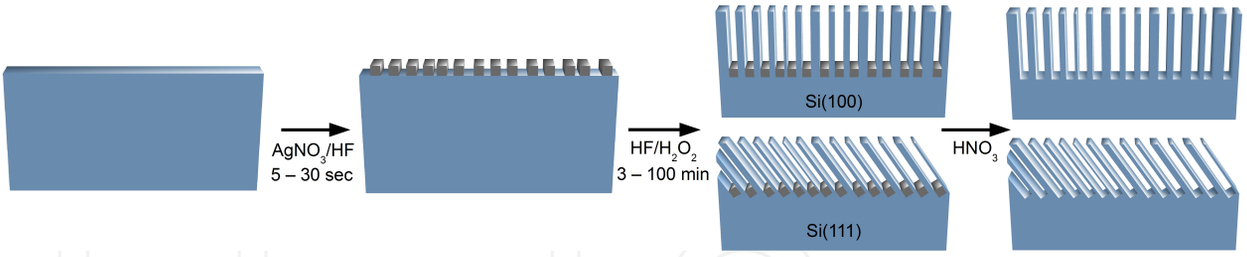

Figure 2. The WCE process is based on a sequence of four solutions starting with oxide removal (solution I: dilute HF, not shown), followed by solution based Ag nanoparticle deposition (solution II), Ag nanoparticle assisted catalytic etching of Si (solution III) and Ag nanoparticle removal (solution IV).

2.2. Fabrication of Semiconductor-Insulator-Semiconductor (SIS) solar cells

SiNWs enable several concepts of efficient solar cell geometries. The charge carrier dividing junction (p-n or Schottky type) can be applied in a radial [23,24] or axial [25,26] concept inside the NWs and a possible solution is also the wrapping of NWs with a second material [27]. In this work, we used a semiconductor-insulator-semiconductor (SIS) heterojunction solar cell concept that has already been developed in the 1970s [28–30]. Therefore, the complex SiNW structure is uniformly coated with a very thin tunneling barrier and a thicker layer of aluminum (Al) doped zinc oxide (ZnO) as a second, transparent wide band gap, degenerately doped semiconductor. In order to achieve this conformal coating, atomic layer deposition (ALD, Oxford Opal) is used. This technique can deposit many materials in a self-limiting process with a thickness control at the Angstrom level even on highly complex surfaces [31,32]. Two different classes of precursors are needed for the ALD deposition of metal oxides like Al_2O_3, TiO_2 or ZnO: metal containing molecules and an oxidizing agent. The two precursors are pulsed into the ALD vacuum chamber one after the other by using very short pulse durations of typically <100ms, while longer inert gas purging steps are used between the precursor pulses to remove residual gas from the chamber. The special advantage of an ALD process is that the precursors are forming a self-limiting monolayer that does not allow further deposition of that precursor. The oxidizing agent can be water or an oxygen plasma which removes the functional groups of the previously deposited metal precursor molecules and forms the metal oxide [33,34]. This step is also self-limiting so that a completed cycle forms a stoichiometric monolayer of the desired material even on 3D surfaces. In the case of Al_2O_3, trimethylaluminum and oxygen plasma were used for its formation and for ZnO deposition, diethylzinc and water pulses are applied. The doping of ZnO with aluminum was realized by substituting every 20^{th} cycle of ZnO by one cycle of Al_2O_3 [35,36].

Two different insulating layer materials were tested to form the barrier layer in the SIS cell: TiO_2 and Al_2O_3. Depending on the material, 10 to 30 Å of the barrier layer were deposited onto the SiNWs. Subsequently, the second semiconductor, Al doped ZnO (AZO), which acts as transparent front contact at the same time, is deposited in the same ALD reactor. The thickness of this layer was typically around 450 nm which resulted in a complete filling of the gaps in between the SiNWs and also created a continuous AZO layer on top of the SiNWs for efficient charge carrier conduction. Figure 3 shows the three steps of the ALD process.

http://dx.doi.org/10.5772/52585

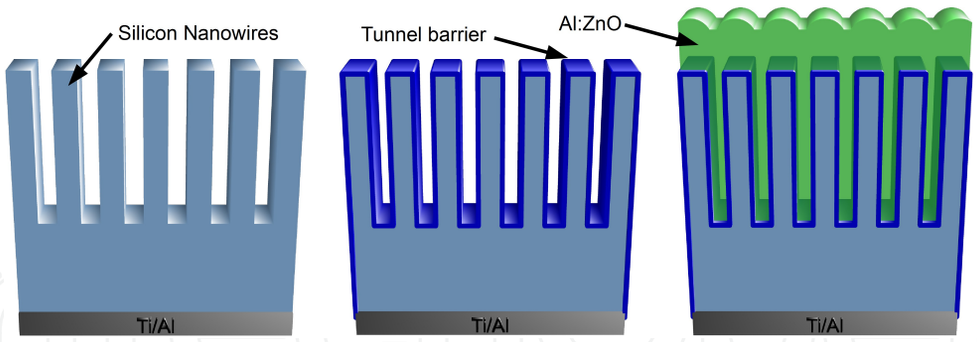

Figure 3. Schematic of the layout of an SIS solar cell concept based on SiNWs: etched SiNWs (left) are coated with a thin tunnel barrier (middle) and subsequently with a transparent front contact – Al doped ZnO (right).

The structural analysis of the completed SIS solar cells was performed by scanning electron microscopy (SEM) techniques including 3D analysis supported by a sequence of focused ion beam (FIB) etching steps. Thereby, the gap filling between SiNWs and SiNW topologies were investigated. Figure 4 shows two colored cross section micrographs of as etched SiNWs and of a completed SIS solar cell that contains wrapping layer stacks on the SiNWs of barrier layer and AZO.

Additionally, the complete SCs were analyzed by glow discharge optical emission spectrometry (GD-OES, Horiba Jobin Yvon JY 5000 RF) to obtain a depth profile of the compositions of the material [37,38]. In a GD plasma source, cathodic sputtering is used to remove material layer-by-layer from a sample surface with an accuracy of a few nanometers [39]. The sample atoms are transported into a plasma plume, in which they are excited and ionized through collisions with electrons, ions and the metastable carrier gas (here: Ar).

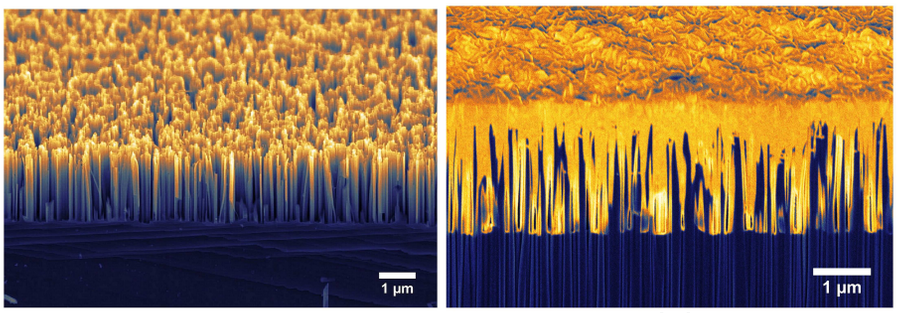

Figure 4. Left: colored SEM micrograph of as etched SiNWs. Right: colored SEM micrograph of a FIB polished cross section of a completed SIS solar cell. The SiNWs (blue) are embedded in barrier layer and Al:ZnO (AZO) (orange).

The analyte isotopes of interest can then be detected via downstream spectroscopic techniques. In the presented study, OES is performed by analyzing the intensities of characteristic emission lines of excited analytes with a spectrometer (typically a Paschen–Runge monochromator or Czerny–Turner polychromator) with A GD-OES Such an analysis was performed on a SiNW SC with a TiO_2 tunnel barrier in the optimization of the solar cell production process. In the SEM profile in Figure 5, the SC can be divided into three regions:

region 1 shows the front contact which solely consists of aluminum doped zinc oxide (AZO). The second region is composed of the SiNW array with a wrapping TiO_2 layer which is filled with AZO. In the third region, the bulk Si wafer is reached. From the measured spectra several interesting information can be extracted [40]. In region 1 the Al content is found to be 2.5 mass% (m%) leading to an ideal conductivity of the AZO layers. In region 2, the silicon content increases only slowly in depth which leads to the assumption that the wires are tapered. This can be interesting for further theoretical investigations regarding optical simulations of light trapping effects. After having checked the residual silver, it is revealed that the cleaning process of the nitric acid did not completely remove the metal. According to these findings, the cleaning process was improved to eliminate residual silver contaminations.

The GD-OES measurements enable another interesting analysis of the silicon nanostructure: Knowing the total mass and thickness of the tunnel barrier layer, the surface of the nanostructures can be calculated. Thereby, the surface enhancement of the etched nanostructures as compared to a flat wafer can be derived. In the case of the TiO_2 barrier SiNW SC (Figure 5), an enhancement factor of 6.2 was calculated. This factor is strongly dependent on the etching conditions and can easily reach values of 40 and more. For a solar cell, a higher surface amount is a clear disadvantage because higher junction areas result in higher surface recombination of charge carriers. On the other hand a higher surface increases the absorption of light and leads to an overall higher charge carrier collection at the interface. Thus, an optimum has to be found between the counteracting mechanisms.

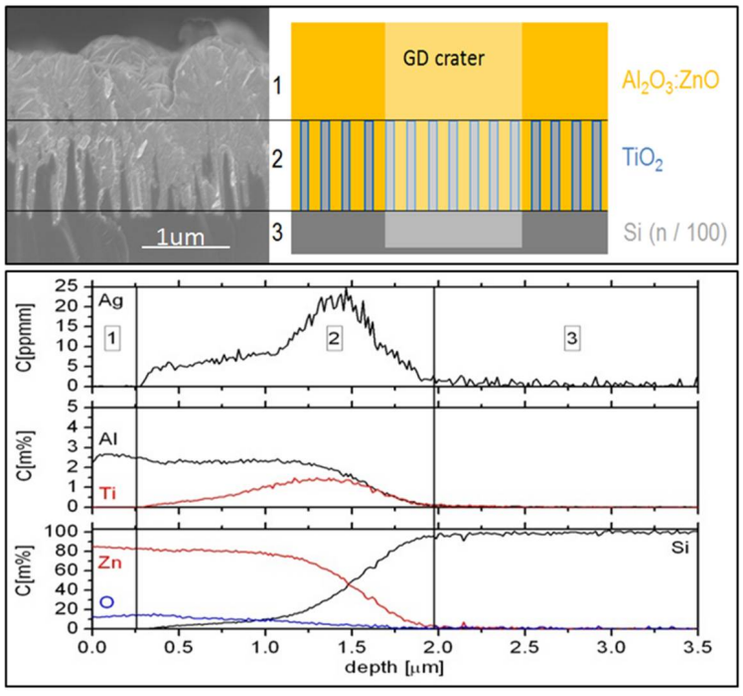

Figure 5. Top: SiNW SC cross section and scheme, showing three different regions inside the cell. Bottom: GD-OES spectra illustrating the depth dependent mass% of the elements Si, O, Zn, Al, Ti and Ag. Adapted from [40].

http://dx.doi.org/10.5772/52585

During the research state, typical SCs had only a size of a few mm² and thus did not need metal front contacts. In the later course of cell development, first demonstrators that had the size to power electrical devices were needed. Therefore, two different prototypes with gold front contact grids and sizes of 36cm² and 1.4cm² were fabricated (see Figure 6). To demonstrate the functionality of the SCs, the small demonstrator was contacted to a motor with a rotating wheel and was illuminated by a battery powered flashlight. Even though the flashlight delivered only a fraction of the sunlight's power, the SC produced enough energy to drive the motor.

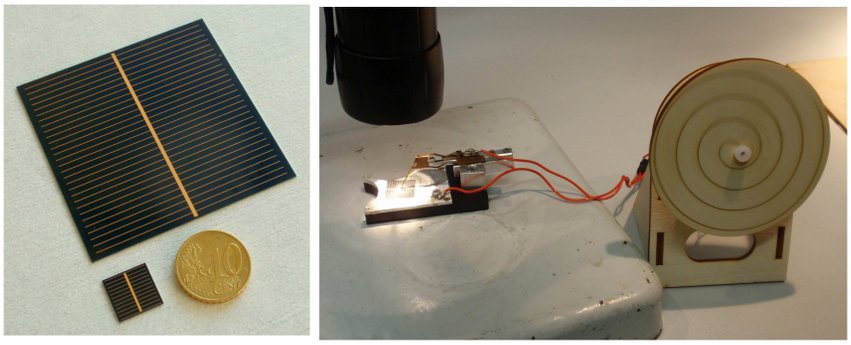

Figure 6. Left: SiNW SC prototypes with gold front contacts. The large cell has a size of 36 cm^2, the small cell measures 1.4 cm^2. For comparison: a 10 €-cent coin. Right: The 1.4 cm^2 cell under a battery-driven flashlight produces enough power to rotate a small toy device.

3. Characterization

The characterization of our fabricated SCs can be divided into investigation of structural and electro-optical properties. Understandably, the conversion efficiency is the most important property. It is determined in a current-voltage (I-V) measurement under a solar simulator that reproduces the certified AM 1.5 solar spectrum. An optical analysis was performed with an integrating sphere in order to investigate the connection between light absorption and efficiency. Figure 7 shows the measured photocurrent under illumination at -2V of 12 different solar cells and the respective optical absorption (mean value between 400 – 1100 nm). In most cases a connection between these two values is clearly visible. Therefore, it is crucial to optimize the absorption by tailoring the nanostructured material composite. Furthermore it can be seen that even a small reduction in absorption from 90% to 88% (wafer 1 and 4) can cause a serious drop in photocurrent from 35 mA to 15 mA. Although other effects may play a role, this effect cannot be neglected.

After these findings the best solar cells were analyzed in detail regarding energy conversion and quantum efficiency as well as local conversion properties in terms of light and electron beam induced current mappings (LBIC/EBIC).

Over 120 solar cells with three different types of Si wafers and 7 different etching conditions were fabricated. For the record cell a n-type Si(111) wafer with a doping of 1-9 Ohm*cm was

used that was etched for 30s/6min in the two etching solutions. The Al_2O_3 tunneling barrier had a thickness of 12 Å. From this cell a small piece of 8mm² size was analyzed in the solar simulator. The SC shows a clearly visible diode-like behavior in the dark with a rectification factor of 6600 at +/-2V. Under AM1.5 illumination the record cell reaches an open circuit voltage V_{OC} of 453 mV, a short circuit current density J_{SC} of 35 mA/cm² and a fill factor (FF) of 57%. This results in a conversion efficiency of 9.1% which is an impressive result for a nanowire based solar cell with as little optimization as we did, e.g. in terms of surface passivation [41,42] or size and shape of the SiNWs [22,43,44]. The corresponding dark and illuminated J-V curves are shown in Figure 8.

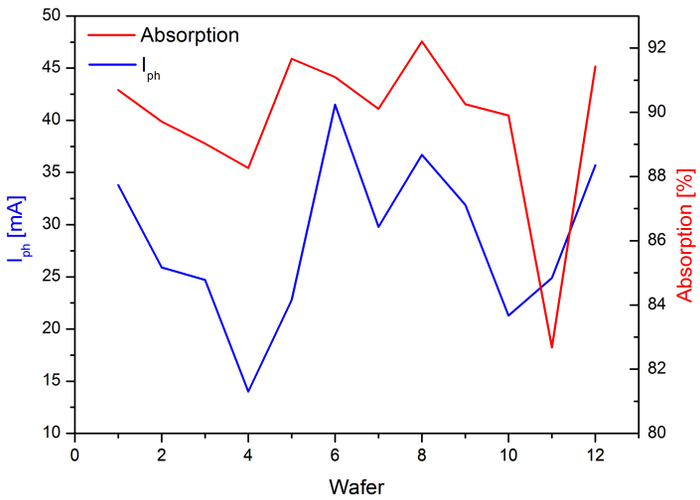

Figure 7. Measured photocurrent (at -2V) and absorption of 12 different solar cells. A correlation is clearly visible.

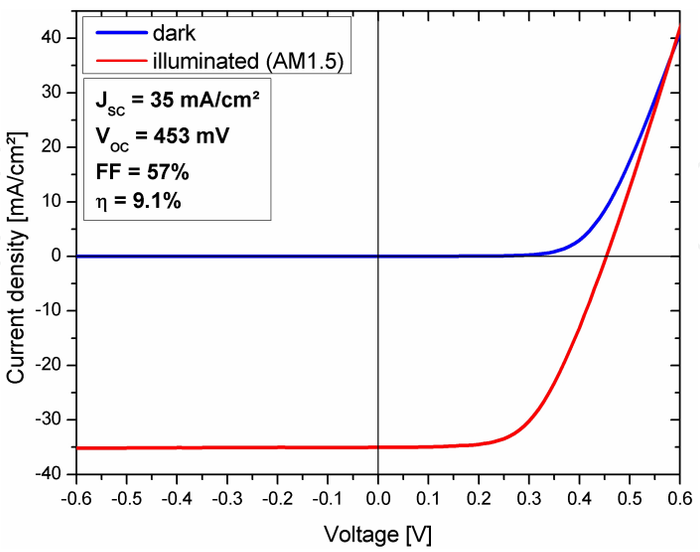

Figure 8. Dark and illuminated current density – voltage (J-V) curves of our record SiNW-SC out of 120 test samples. Very high J_{SC} combined with average V_{OC} and fill factor yield in a conversion efficiency of 9.1%.

http://dx.doi.org/10.5772/52585

3.1. Local electro-optical properties

To determine the influence of structural inhomogeneity on the electrical properties, it is necessary to generate localized charge carriers inside the solar cell and perform a mapping across the cell while monitoring the generated external current between front and back contacts. Two different methods enable such an analysis: light and electron beam induced current (LBIC [45] & EBIC [25, 46]) measurements. In LBIC, a laser is scanned over the solar cell surface and the generated current is measured for each spot. In this way an efficiency mapping can be obtained. By using lasers with different wavelengths the response of the solar cell to distinct excitation energies can be investigated. Furthermore, an external quantum efficiency (EQE) mapping can be calculated from such a measurement. The disadvantage of LBIC is its large laser spot focus which inhibits the analysis of μm-sized defects. Here EBIC becomes suitable. The electron beam of an SEM can be focused on a few nm and with a low acceleration voltage the expansion of excited charge carriers can be kept at a minimum of <100nm. Every incident electron generates thousands of charge carrier pairs that can be separated by the nearby SIS junction. This enables the visualization of the internal charge carrier separation at the SiNW - front contact interface.

The LBIC and EBIC analyses were performed on the 1.4 cm^2 prototypes with metal front grid shown in Figure 6. For the LBIC measurements, a custom built system with four different lasers with wavelengths of 405, 544, 633 and 1064 nm was applied. Figure 9 shows the mapping results and an EBIC mapping of the same cell as well in order to be able to draw a comparison. The LBIC mappings are normalized to show the dependence of the power output on the light wavelength. Nearly no current is generated at 405 nm. At 544 nm, several areas are visible that have better or worse efficiency. These areas arise from an inhomogeneous etching process which generates areas with slightly higher or lower absorption. At 633 nm two small areas reach a generated current of 25 μA. Visible for the naked eye, these areas appear darker than the remaining surface. At 1064 nm, the light is not absorbed in the SiNWs themselves anymore but in the bulk wafer below. Therefore the signal is very homogeneous as the nanowires do not influence the current generation anymore. The EBIC mapping can be compared best with the 633 nm LBIC mapping. Due to the higher resolution of the EBIC, this measurement shows much more details.

In order to explain the different current amounts in the LBIC measurements in a better way, the EQE of the SC was measured. The results are shown in Figure 10. The wavelength-dependent behavior is in accordance with the determined LBIC mappings. At 405 nm, the EQE is at nearly zero and 633 nm exhibits the highest EQE from all four laser wavelengths. Although the EQE curve is similar in shape to typical commercial solar cell EQE results, only lower values are reached. The reasons are still under investigation. Furthermore, Figure 10 shows the optical absorption of the SC which was calculated by 1 minus the measured total reflectance. In Figure 11, a high resolution large scale EBIC scan of a SC demonstrator is shown. The simultaneously gathered SEM and EBIC signals are coded in brown and green color schemes. The EBIC signal clearly shows regions of lower or higher current due to etching variations and also many circular defects which

seem to be the result of pinholes in the tunnel barrier layers. In several circular defects, a dirt particle in the middle seems to be the cause of the short circuit.

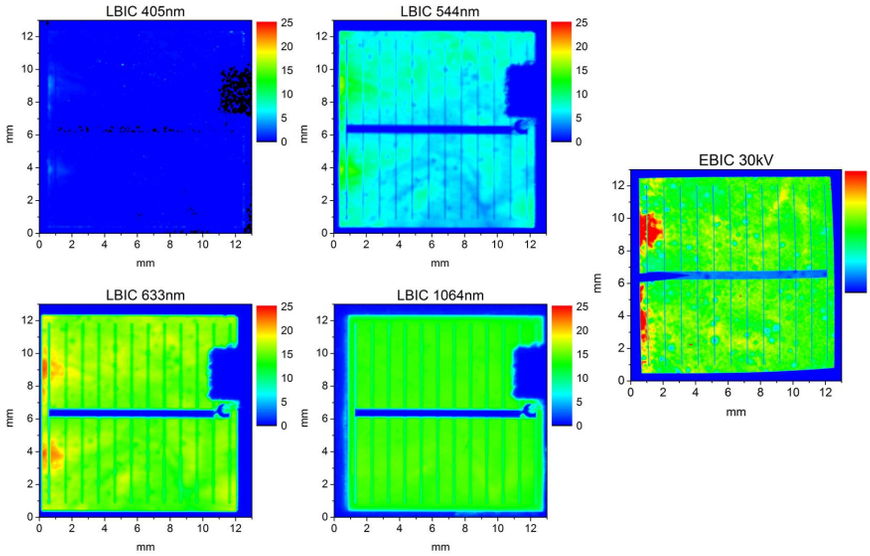

Figure 9. LBIC mapping at four different laser wavelengths and the corresponding EBIC measurement at 30 kV accelerating voltage. The inactive region in the top-right of each LBIC measurement is caused by shading from the mounting.

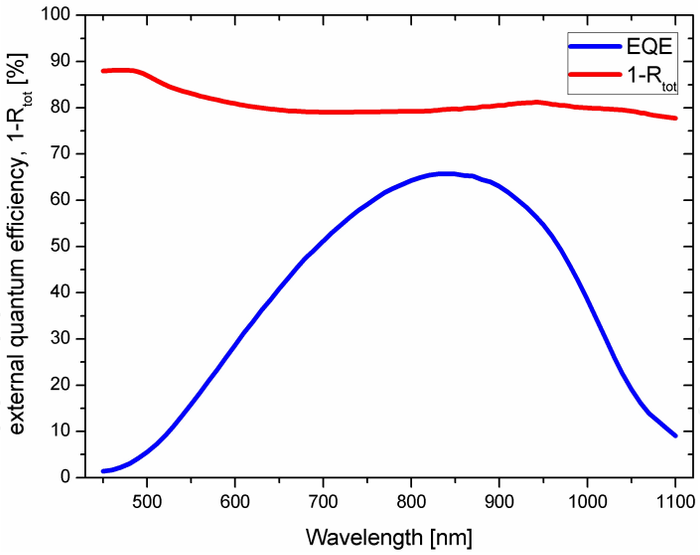

Figure 10. Absorption ($1\text{-}R_{tot}$) and EQE of a SiNW-based solar cell prototype.

The EBIC measurement is a powerful tool not only for observing the surface of a solar cell but also for looking inside the cell when combining sequences of EBIC analyses and FIB sectioning and polishing. Combined with a focused ion beam (FIB), information on sub-surface structures can be obtained. In a tomographic approach, a section into the SiNW based SC is

http://dx.doi.org/10.5772/52585

carried out and a sub-surface slice of a few μm in depth and length is polished. The prepared area can subsequently be investigated by EBIC mapping and typical SEM SE imaging. Further slicing and polishing and repeated EBIC analysis permit a 3D reconstruction of EBIC as well as SE data resulting in tomographic information. Figure 12 represents the concept of a cross sectional EBIC measurement: The electron beam scans over the ion beam polished cross section of a SiNW based SIS SC and the current that flows between the front and back contact is amplified and mapped by using the electron beam position. A resulting image is also shown.

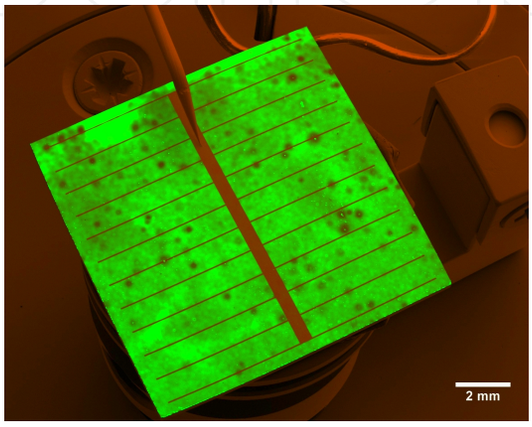

Figure 11. A large scale combined SEM/EBIC image of a solar cell surface. Point defects appear as darker dots and larger sized contrast differences indicate structural variations due to inhomogeneous etching.

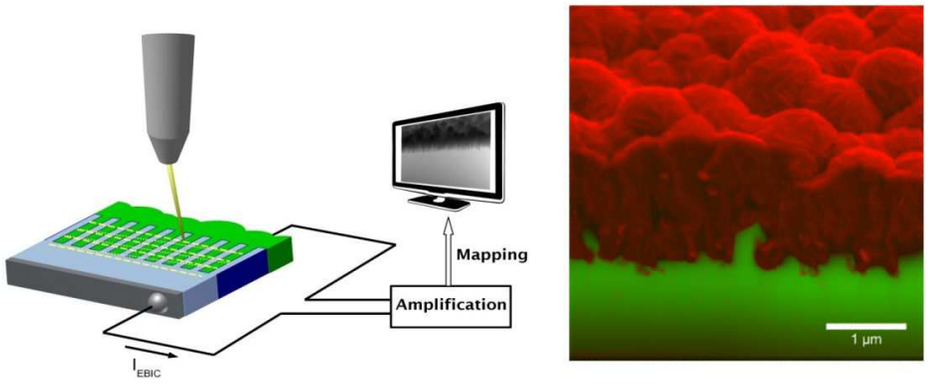

Figure 12. Left: Scheme of a cross sectional EBIC measurement of a SiNW based SIS SC. Right: colored dual-signal micrograph that shows the SEM image in red and the EBIC in green. A pronounced EBIC current of an individual SiNW is clearly visible in green.

The 3D-EBIC is devoted to solve an important question in the field of SiNW solar cells: Are the nanowires active photovoltaic components or do they only act as passive anti-reflecting building blocks? It is generally accepted that SiNWs absorb light by generating charge carrier pairs [10]. However, whether it is possible to separate electrons and holes prior to their recombination is a question to be answered for each and every material and cell concept

again. To answer these interesting and important questions a dual beam SEM/FIB system (Tescan Lyra 3) with an integrated quantitative EBIC detector (Point electronic and Kammrath & Weiss) is used. The gallium ion beam of the FIB cuts a volume of 10x10x10 μm^3 of the solar cell perpendicular to the surface slice by slice. The electron beam observes each slice from an angle of 55° to the perpendicular and creates a secondary electron image as well as an EBIC image. Afterwards, these images can be combined in order to create a 3D reconstruction of the solar cell. In Figure 13, three slices of a 3D reconstruction are displayed. The assembled dataset offers a multitude of visualizations which can be shown best in a video. Therefore, the microscopy manufacturer Tescan provides a video of the analysis of our SiNW-SIS-SC which can be viewed via this internet link: http://www.youtube.com/watch?v=X9O6pwcN4Tg. It shows the possibilities in signal combination as well as the visualization of complex 3D surfaces.

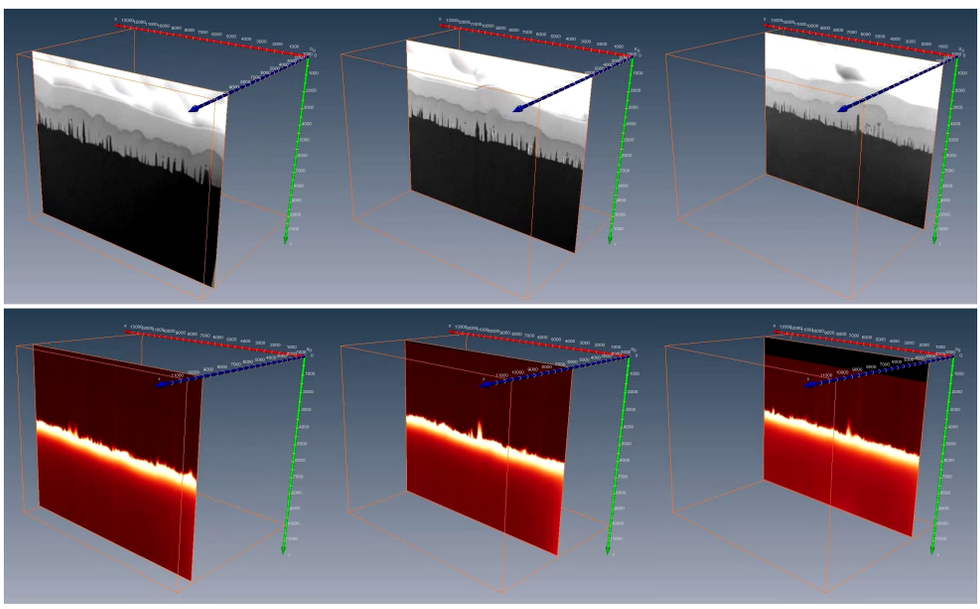

Figure 13. Three single slices out of 400 that show the SE-signal (top) as well as the EBIC signal (bottom) at the same position.

The 3D determination of electrical properties becomes very important in times of emerging nanostructured solar cells. Our results which are shown in Figure 12 and 13, prove that nanowires can be active photovoltaic components. This can be seen in the second slice where a single nanowire is visible in the EBIC image. Otherwise, many NWs are visible in the SEM image that cannot be seen in the EBIC signal. The difference between active and passive PV component seems to lie in the diameter of the wire. NWs, which are smaller than 50nm, exhibit no EBIC signal. That can be explained by the high surface to volume ratio, which leads to higher recombination, or a lesser absorption and thus no charge carrier generation occurs. These information are of great value when it comes to further optimization of the initial etching process. The nanowire dimensions should be in an area where high absorption is still achieved and charge carrier separation can take place inside the wires.

http://dx.doi.org/10.5772/52585

4. Outlook on nanowire research

The field of nanowire based solar cell research develops very fast and thus new methods and materials are coming up continuously. Our group is driving this type of research forward very actively and we are even constantly improving our own records. This outlook will give the reader some ideas about the progress of NW cell research in our lab. By further improving nanowire based cell concepts, we are aiming to achieve the goal of seeing these cells on top of a roof one day.

4.1. Silicon nanowire arrays formed by reactive ion etching

Reactive ion etching (RIE) in combination with nanosphere lithography (NSL) represents a new way of forming hexagonal arrays of SiNWs with controllable geometries in wafers [22] or even multicrystalline silicon (mc-Si) thin films on glass. [44] These structures offer several advantages regarding further systematic research on SiNW based optoelectronic and solar cell devices. Since device constituting properties like spectral absorption, reflection and the area and distribution of charge separating surfaces (p/n-junctions, heterojunctions etc.) are dependent on SiNW array geometries, a control of these geometries creates the opportunity for systematic device development. Figure 14 shows an example of the potential of this highly flexible and scalable process which results in large areas of nanostructured surfaces. The nanospheres arrange in self-aligned hexagonal colloidal 2D crystals on the wafer surface. The initial sphere diameter determines the lattice constant of the structure, whereas oxygen-plasma reduced spheres pre-determine the diameter of the SiNWs.

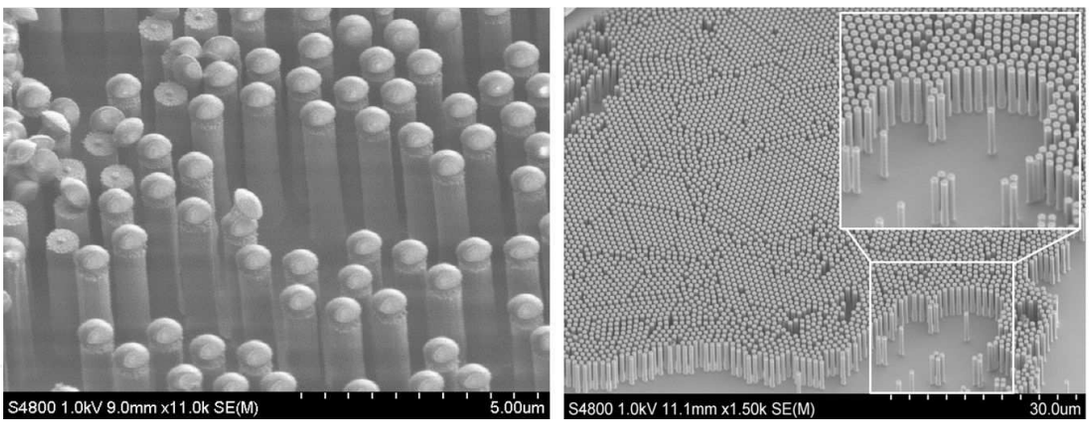

Figure 14. Left: RIE of a NSL patterned wafer surface. The nanospheres act as a shadow mask for the RIE process which results in aligned arrays of SiNWs. Inset: The lattice constant of the hexagonal arrays is pre-determined by the initial sphere diameter d_i, the diameter of the structures d_r can be controlled by the reduction of the initial spheres. Right: With the described method, the structuring of large surfaces is possible as it can be seen in the SEM micrograph.

RIE etched SiNWs may not offer the high throughput and cheap production of WCE NWs, but the predefined non-random structure offers many advantages in the control of optical and electrical properties in NW SCs compared to the random structures of chemically etch-

ed NWs and thus permit tailoring and optimizing SC efficiencies. Moreover, the etched SiNWs usually have a smaller surface to volume ratio, thus permitting smaller surfaces that need passivation [41].

4.2. Novel electrodes based on silver nanowires or graphene

One-dimensional (1D) metal nanostructures, especially single crystalline nanowires, have attracted intensive interest because of their great potential for practical applications in nanoscale electronics, optoelectronics, and molecular sensing devices. However, one of the most significant challenges still facing device fabrication and processing is the large scale reproducibility of the nanowires into highly controlled arrays with high uniformity. Herein, we demonstrate an extremely simple method for large-scale and highly ordered silver nanowire (AgNW) monolayer synthesis via a thermal assembling process. These AgNWs offer new possibilities in the formation of transparent and highly conductive contacts.

The AgNW were synthesized by wet chemistry. For a typical synthesis, 5 ml of ethylene-glycol (EG) was heated to 175±10 °C for 1 h under magnetic stirring. Subsequently, Cu-additive solution (40 μL, 4 mM $CuCl_2$) was injected together with the polymer PVP (1.5 ml with a concentration of 0.147 M) into the heated EG. The volume, systematically influences can design the final shape and size of the AgNW. Finally, 1.5 ml of a 0.094 M $AgNO_3$ was injected slowly (for 10min). After 1 to 1.5 h, the reaction was stopped and cooled to room temperature by a water bath. Products were then washed with ethanol three times.

SEM images with low and high magnification of Ag nanowires (AgNW) are presented in Figure 15. The AgNW had a typical length of 30±10 μm, with diameter of 50±10 nm.

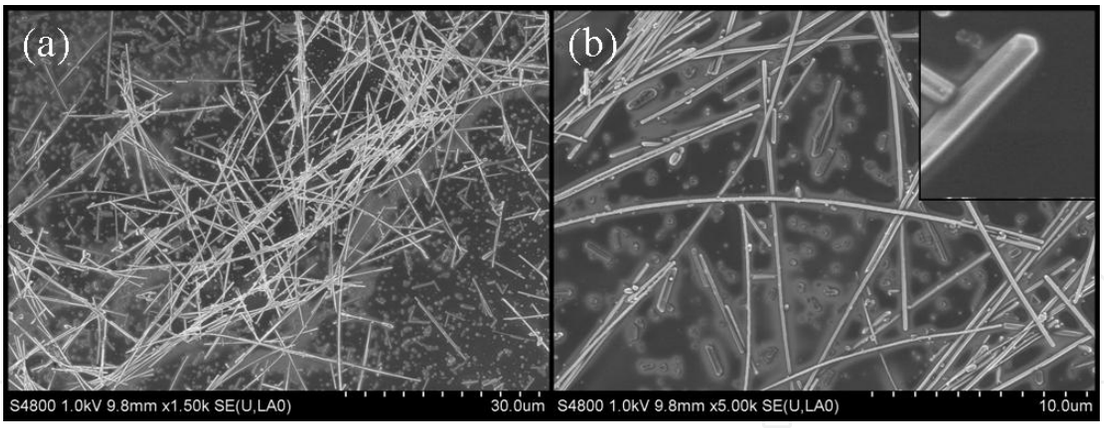

Figure 15. SEM micrographs of AgNW prepared by thermal assembly in the presence of PVP polymer. (a) A low-magnification SEM image reveals the highly uniform shape of AgNWs, (b) A higher magnification SEM image shows the high aspect ratio of AgNW. Inset is a SEM image that illustrates the pentagonal cross-section of the AgNWs.

Graphene with its outstanding optical and electrical properties offers many advantages when applied as contact material to SiNW SCs. The high in-plane conductivity as well as the high optical transparency recommends graphene as a new type of TCMs (transparent conductive materials) and it might substitute or support the typical TCO in our SiNW SC concept. It can be easily transferred to desired surfaces and its flexibility offers advantag-

http://dx.doi.org/10.5772/52585

es for flexible SCs (e.g. on plastic substrates or metal foils). Figure 16 shows a transferred layer of graphene on top of RIE fabricated SiNWs. Preliminary investigations strongly promise excellent contact properties and thus research on this material will be forced with a lot of effort.

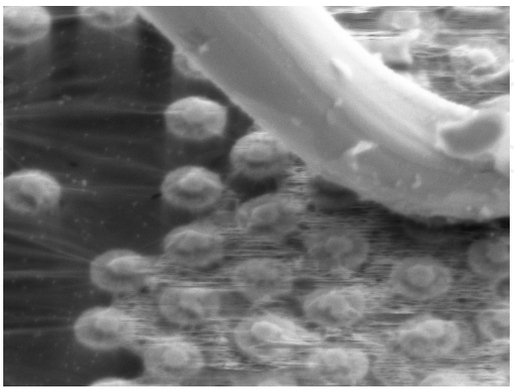

Figure 16. A graphene monolayer was deposited on top of SiNWs that are created by RIE to act as front contact. In the upper part the contact needle of the EBIC module can be seen.

5. Conclusions and outlook

In the last years not only have we developed and realized a novel nanowire based solar cell concept, but we have also developed advanced analysis methods for such kind of nanostructured devices. By systematically using cheap and abundant materials and avoiding expensive vacuum equipment for the nanostructuring process, we generated solar cells with over 9% conversion efficiency. As these values are the results of early stage research, further improvement up to an efficiency of 12-15% are expected. Furthermore, the concept will be transferred to thin films like multicrystalline silicon on glass or flexible substrates.

The development of 3D-EBIC will be most likely of great influence for the analysis of 3-dimensional nanostructured solar cells and thus it is also a great advance for the PV research field.

Acknowledgements

The authors gratefully acknowledge Florian Talkenberg for the ALD processes, Arne Bochmann for the LBIC measurements and Maria Hadjipanayi for the EQE investigations. Many thanks go to Gerald Brönstrup and Felix Voigt for fruitful discussions.

The authors gratefully acknowledge financial support by the European Commission projects within the framework of FP7, “ROD-SOL” and “Fiblys”.

Author details

Björn Hoffmann[1,2], Vladimir Sivakov[2], Sebastian W. Schmitt[1], Muhammad Y. Bashouti[1], Michael Latzel[1], Jiří Dluhoš[3], Jaroslav Jiruse[3] and Silke Christiansen[1,2]

1 Max Planck Institute for the Science of Light, TDSU Photonic Nanostructures, Erlangen, Germany

2 Institute of Photonic Technology, Department Semiconductor Nanostructures, Jena, Germany

3 TESCAN, a.s., Brno, Czech Republic

References

[1] Green MA. (2001) Third generation photovoltaics: Ultra-high conversion efficiency at low cost. Prog Photovolt Res Appl. 9(2),123-35. http://doi.wiley.com/10.1002/pip.360

[2] Kaufmann CA, Neisser A, Klenk R, Scheer R. (2005) Transfer of Cu(In,Ga)Se2 thin film solar cells to flexible substrates using an in situ process control. Thin Solid Films. 480-481,515-9. http://dx.doi.org/10.1016/j.tsf.2004.11.067

[3] Green MA, Emery K, Hishikawa Y, Warta W, Dunlop ED. (2012) Solar cell efficiency tables (version 39). Prog Photovolt Res Appl. 20(1),12–20. http://onlinelibrary.wiley.com/doi/10.1002/pip.2163/full

[4] Bagnall DM, Boreland M. (2008) Photovoltaic technologies. Energy Policy. 36(12), 4390–6. http://linkinghub.elsevier.com/retrieve/pii/S0301421508004552

[5] Du QG, Kam CH, Demir HV, Yu HY, Sun XW. (2011) Broadband absorption enhancement in randomly positioned silicon nanowire arrays for solar cell applications. Opt Lett. 36(10),1884–6. http://www.ncbi.nlm.nih.gov/pubmed/21593923

[6] Tsakalakos L, Balch J, Fronheiser J, Shih M-Y, LeBoeuf SF, Pietrzykowski M, et al. (2007) Strong broadband optical absorption in silicon nanowire films. J Nanophotonics. 1(1),013552. http://link.aip.org/link/JNOACQ/v1/i1/p013552/s1&Agg=doi

[7] Srivastava SK, Kumar D, Singh PK, Kar M, Kumar V, Husain M. (2010) Excellent antireflection properties of vertical silicon nanowire arrays. Sol. Energy Mater. Sol. Cells. 94(9),1506–11. http://linkinghub.elsevier.com/retrieve/pii/S0927024810000863

[8] Srivastava SKSK, Kumar D, Singh PKP, Kar M, Kumar V, Husain M. (2011) Fabrication of silicon nanowire arrays based solar cell with improved performance. Sol. Energy Mater. Sol. Cells. 95(1),215–8. http://linkinghub.elsevier.com/retrieve/pii/S092702481000214X

[9] Sivakov V, Andrä G, Gawlik A, Berger A, Plentz J, Falk F, et al. (2009) Silicon nanowire-based solar cells on glass: synthesis, optical properties, and cell parameters. Nano Lett. 9(4),1549–54. http://dx.doi.org/10.1021/nl803641f

[10] Brönstrup G, Garwe F, Csáki A, Fritzsche W, Steinbrück A, Christiansen S. (2011) Statistical model on the optical properties of silicon nanowire mats. Phys. Rev., B. 84(12),1–10. http://link.aps.org/doi/10.1103/PhysRevB.84.125432

[11] Cao L, White JS, Park J-S, Schuller J a, Clemens BM, Brongersma ML. (2009) Engineering light absorption in semiconductor nanowire devices. Nat Mater. 8(8),643–7. http://www.ncbi.nlm.nih.gov/pubmed/19578337

[12] Xie WQ, Oh JI, Shen WZ. (2011) Realization of effective light trapping and omnidirectional antireflection in smooth surface silicon nanowire arrays. Nanotechnology. 22(6),065704. http://www.ncbi.nlm.nih.gov/pubmed/21212474

[13] Muskens OL, Rivas JG, Algra RE, Bakkers EP a M, Lagendijk A. (2008) Design of light scattering in nanowire materials for photovoltaic applications. Nano Lett. 8(9), 2638–42. http://www.ncbi.nlm.nih.gov/pubmed/18700806

[14] Wagner R, Ellis W. (1964) Vapor-Liquid-Solid Mechanism of Single Crystal Growth. Appl Phys Lett. 4(5),89–90. http://ieeexplore.ieee.org/xpls/abs_all.jsp?arnumber=4850930

[15] Hofmann S, Ducati C, Neill RJ, Piscanec S, Ferrari a. C, Geng J, et al. (2003) Gold catalyzed growth of silicon nanowires by plasma enhanced chemical vapor deposition. J Appl Phys. 94(9),6005. http://link.aip.org/link/JAPIAU/v94/i9/p6005/s1&Agg=doi

[16] Sunkara MK, Sharma S, Miranda R, Lian G, Dickey EC. (2001) Bulk synthesis of silicon nanowires using a low-temperature vapor–liquid–solid method. Appl Phys Lett. 79(10),1546. http://link.aip.org/link/APPLAB/v79/i10/p1546/s1&Agg=doi

[17] Peng K, Fang H, Hu J, Wu Y, Zhu J, Yan Y, et al. (2006) Metal-particle-induced, highly localized site-specific etching of Si and formation of single-crystalline Si nanowires in aqueous fluoride solution. Chemistry. 12(30),7942–7. http://www.ncbi.nlm.nih.gov/pubmed/16871502

[18] Sivakov V, Bro◎nstrup G, Pecz B, Berger a., Radnoczi GZ, Krause M, et al. (2010) Realization of Vertical and Zigzag Single Crystalline Silicon Nanowire Architectures. J Phys Chem C. 114(9),3798–803. http://pubs.acs.org/doi/abs/10.1021/jp909946x

[19] Huang Z, Geyer N, Werner P, de Boor J, Gösele U. (2011) Metal-assisted chemical etching of silicon: a review. Advanced Materials. 23(2),285–308. http://doi.wiley.com/10.1002/adma.201001784

[20] Sivakov V, Voigt F, Hoffmann B, Gerliz V, Christiansen S. (2011) Wet - Chemically Etched Silicon Nanowire Architectures◎: Formation and Properties. In: Hashim A, editor. Nanowires - Fundamental Research. Intech; 2011. p. 45 - 80.http://www.intechopen.com/articles/show/title/wet-chemically-etched-silicon-nanowire-architectures-formation-and-properties

[21] Huynh WU, Dittmer JJ, Alivisatos AP. (2002) Hybrid nanorod-polymer solar cells. Science (80-). 295(5564),2425–7. http://www.sciencemag.org/content/295/5564/2425.abstract

[22] Garnett E, Yang P. (2010) Light trapping in silicon nanowire solar cells. Nano Lett. 10(3),1082–7. http://www.ncbi.nlm.nih.gov/pubmed/20108969

[23] Garnett EC, Yang P. (2008) Silicon nanowire radial p-n junction solar cells. J. Am. Chem. Soc. 130(29),9224–5. http://www.ncbi.nlm.nih.gov/pubmed/18576622

[24] Ke Y, Wang X, Weng XJ, Kendrick CE, Yu YA, Eichfeld SM, et al. (2011) Single wire radial junction photovoltaic devices fabricated using aluminum catalyzed silicon nanowires. Nanotechnology. 22(44),445401. http://www.ncbi.nlm.nih.gov/pubmed/21983364

[25] Hoffmann S, Bauer J, Ronning C, Stelzner T, Michler J, Ballif C, et al. (2009) Axial p-n junctions realized in silicon nanowires by ion implantation. Nano Lett. 9(4),1341–4. http://www.ncbi.nlm.nih.gov/pubmed/19256535

[26] Wen C-Y, Reuter MC, Bruley J, Tersoff J, Kodambaka S, Stach EA, et al. (2009) Formation of compositionally abrupt axial heterojunctions in silicon-germanium nanowires. Science (80-). 326(5957),1247–50. http://www.ncbi.nlm.nih.gov/pubmed/19965471

[27] Tsai S-H, Chang H-C, Wang H-H, Chen S-Y, Lin C-A, Chen S-A, et al. (2011) Significant Efficiency Enhancement of Hybrid Solar Cells Using Core-Shell Nanowire Geometry for Energy Harvesting. ACS Nano., 5(12), 9501-10. http://pubs.acs.org/doi/abs/10.1021/nn202485m

[28] Shewchun J, Dubow J, Myszkowski A, Singh R. (1977) The operation of the semiconductor-insulator-semiconductor (SIS) solar cell: Theory. J Appl Phys. 49(2),855–64. http://ieeexplore.ieee.org/xpls/abs_all.jsp?arnumber=5104464

[29] Shewchun J, Dubow J, Wilmsen C, Singh R, Burk D, Wager J. (1978) The operation of the semiconductor-insulator-semiconductor solar cell: Experiment. J Appl Phys. 50(4),2832–9. http://ieeexplore.ieee.org/xpls/abs_all.jsp?arnumber=5105997

[30] Genis AP, Smith PA, Emery K, Singh R, DuBow JB. (1980) Efficient indium tin oxide/polycrystalline silicon semiconductor-insulator-semiconductor solar cells. Appl Phys Lett. 37(1),77. http://link.aip.org/link/APPLAB/v37/i1/p77/s1&Agg=doi

[31] Ritala M, Leskela M. (2001) Atomic layer deposition. Handbook of thin film materials. 1,103–59. http://cambridgenano.com/papers/atomic layer deposition ritala leskela.pdf

[32] Leskelä M, Ritala M. (2002) Atomic layer deposition (ALD): from precursors to thin film structures. Thin Solid Films. 409(1),138–46. http://linkinghub.elsevier.com/retrieve/pii/S0040609002001177

[33] Dingemans G, Seguin R, Engelhart P, Sanden MCMVD, Kessels WMM. (2010) Silicon surface passivation by ultrathin Al 2 O 3 films synthesized by thermal and plasma

atomic layer deposition. Phys. Status Solidi RRL. 4(1-2),10–2. http://doi.wiley.com/10.1002/pssr.200903334

[34] Profijt HB, Potts SE, van de Sanden MCM, Kessels WMM. (2011) Plasma-Assisted Atomic Layer Deposition: Basics, Opportunities, and Challenges. J Vac Sci Technol A. 29(5),050801. http://link.aip.org/link/JVTAD6/v29/i5/p050801/s1&Agg=doi

[35] Saarenpää H, Niemi T, Tukiainen A, Lemmetyinen H, Tkachenko N. (2010) Aluminum doped zinc oxide films grown by atomic layer deposition for organic photovoltaic devices. Sol. Energy Mater. Sol. Cells. 94(8),1379–83. http://linkinghub.elsevier.com/retrieve/pii/S0927024810001716

[36] Yamada A, Sang B, Konagai M. (1997) Atomic layer deposition of ZnO transparent conducting oxides. Appl Surf Sci. 112,216–22. http://linkinghub.elsevier.com/retrieve/pii/S0169433296010227

[37] Angeli J, Bengtson A, Bogaerts A, Hoffmann V, Hodoroaba V-D, Steers E. (2003) Glow discharge optical emission spectrometry: moving towards reliable thin film analysis: a short review. J Anal At Spectrom. 18(6),670. http://pubs.rsc.org/en/content/articlehtml/2003/ja/b301293j

[38] Schmitt SW, Gamez G, Sivakov V, Schubert M, Christiansen SH, Michler J. (2011) Chemical and optical characterisation of atomic layer deposition aluminium doped ZnO films for photovoltaics by glow discharge optical emission spectrometry. J Anal At Spectrom. 26(4),822. http://xlink.rsc.org/?DOI=c0ja00158a

[39] Pisonero J, Fernández B, Pereiro R, Bordel N, Sanz-Medel A. (2006) Glow-discharge spectrometry for direct analysis of thin and ultra-thin solid films. Trends Analyt Chem. 25(1),11–8. http://dx.doi.org/10.1016/j.trac.2005.04.019

[40] Schmitt SW, Venzago C, Hoffmann B, Sivakov V, Hofmann T, Michler, J., Christiansen, S. Gamez G. (2012) Glow discharge techniques in the chemical analysis of photovoltaic materials. Prog Photovolt Res Appl. http://doi.wiley.com/1021002/pip.2264.

[41] Bashouti MY, Stelzner T, Berger A, Christiansen S, Haick H. (2008) Chemical Passivation of Silicon Nanowires with C 1 –C 6 Alkyl Chains through Covalent Si–C Bonds. J Phys Chem C. 112(49),19168–72. http://dx.doi.org/10.1021/jp8077437

[42] Dan Y, Seo K, Takei K, Meza JH, Javey A. (2011) Dramatic reduction of surface recombination by in situ surface passivation of silicon nanowires. Nano Lett. 11(6) 2527 http://pubs.acs.org/doi/abs/10.1021/nl201179n

[43] Kim DR, Lee CH, Rao PM, Cho IS, Zheng X. (2011) Hybrid Si Microwire and Planar Solar Cells: Passivation and Characterization. Nano Lett. 11(7), 2704 http://www.ncbi.nlm.nih.gov/pubmed/21609002

[44] Schmitt SW, Schechtel F, Amkreutz D, Bashouti M, Srivastava, S. K., Hoffmann B, Rech B, et al. (2012) Nanowire arrays in multi-crystalline silicon thin films on glass: a promising material for photovoltaics, opto-electronics and fundamental research in nano-technology. Nano Lett. 12(8), 4050.

[45] Bajaj J, Tennant WE. (1990) Remote contact LBIC imaging of defects in semiconductors. J Cryst Growth. 103(1-4),170–8. http://www.sciencedirect.com/science/article/pii/002202489090186O

[46] Donolato C. (1983) Theory of beam induced current characterization of grain boundaries in polycrystalline solar cells. J Appl Phys. 54(3),1314. http://link.aip.org/link/JAPIAU/v54/i3/p1314/s1&Agg=doi

IntechOpen